CCS Chemistry

RESEARCH ARTICLE

Received: June 23, 2020 | Accepted: Oct. 21, 2020 | Published: Dec. 4, 2020

Manipulation of Molecular Qubits by Isotope Effect on Spin Dynamics

Jing Li[1], Shi-Jie Xiong[2], Chun Li[3], Biaobing Jin[3], Yi-Quan Zhang[4], Shang-Da Jiang[5], Zhong-Wen Ouyang[6], Zhenxing Wang[6]*, Xing-Long Wu[2]*, Johan van Tol[7]* & You Song[1]*

[1]*State Key Laboratory of Coordination Chemistry, School of Chemistry and Chemical Engineering, Nanjing University, Nanjing 210023,* [2]*National Laboratory of Solid State Microstructures, Department of Physics, Nanjing University, Nanjing 210093,* [3]*Research Institute of Superconductor Electronics (RISE), School of Electronic Science and Engineering, Nanjing University, Nanjing 210093,* [4]*Jiangsu Key Laboratory for NSLSCS, School of Physical Science and Technology, Nanjing Normal University, Nanjing 210023,* [5]*National Laboratory for Molecular Sciences, State Key Laboratory of Rare Earth Materials Chemistry and Applications, Beijing Key Laboratory for Magnetoelectric Materials and Devices, College of Chemistry and Molecular Engineering, Peking University, Beijing 100871,* [6]*Wuhan National High Magnetic Field Center & School of Physics, Huazhong University of Science and Technology, Wuhan 430074,* [7]*National High Magnetic Field Laboratory, Florida State University, Tallahassee, FL 32310*

**Corresponding authors:* yousong@nju.edu.cn; hkxlwu@nju.edu.cn; zxwang@hust.edu.cn; vantol@magnet.fsu.edu

Cite this: *CCS Chem.* **2020**, *2*, 2548–2556

Controlling spin behavior via external stimuli is a key route to develop molecular spintronics devices. Photons, temperature, pressure, chemicals, and electric field are the possible stimuli. Herein, we report a new method, the isotope effect, to control spin behavior in molecule magnet systems. It can not only control the relaxation of magnetization, but also regulate the spin lifetime of quantum coherence. In this regard, we found a couple of low-spin Co(II) complexes, {[CoL](CH$_3$CN)}[BPh$_4$]$_2$·CH$_3$CN (1-H; L = 1,5-bis(2pyridylmethyl)-1,5-diazacyclooctane) and its deuterated analog {[CoL](CD$_3$CN)}[BPh$_4$]$_2$·CD$_3$CN (1-D), exhibiting the rare ON/OFF switching of double spin relaxation behaviors in magnetic relaxation as well as the regulation of spin lifetime in quantum coherence at low temperatures. We discuss the mechanisms underlying the formation and the relevance of intramoleculer vibration modes, which give the direct experimental evidence of spin–intramolecular vibration coupling, and also provide new guidance for the ultrafast and electrical control of spin behaviors.

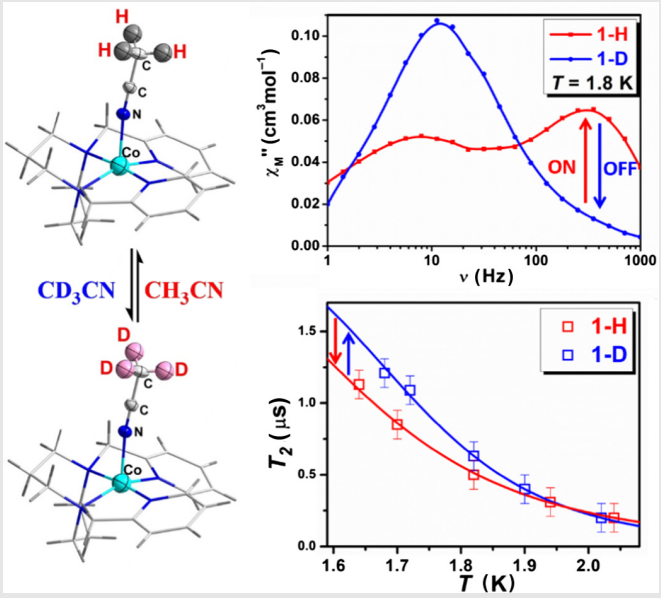

Keywords: molecule-based magnetism, molecular qubits, isotope effect, spin–vibration coupling, quantum coherence

DOI: 10.31635/ccschem.020.202000384
Citation: *CCS Chem.* **2020**, 2, 2548–2556
Citation denotes calendar and volume year of first online publication.
Issue Assignment: Volume 3 (2021), Issue 9

Introduction

Single-molecule magnets (SMMs)[1] and molecule-based spin quantum bits (qubits)[2,3] are promising candidates for the development of nanospintronic[4] and quantum computing,[5] which may bring opportunities for the second quantum revolution. The spin-relaxation times T_1 and T_2 are the crucial factors to evaluate the performance of SMMs and qubits in applications.[6] One of the key issues is to better understand the mechanism of T_1 and T_2 in the spin relaxation of magnetic systems. This may take place due to the internal nuclear spin fluctuations,[7] the spin flip-flop processes,[8–11] molecular symmetry,[12] spin–phonon coupling,[13–17] and so forth. Among them, the first three are fully studied, but the connotation of spin–phonon coupling is not clear enough as of now.

In general, phonons are generated by periodic lattice vibrations or intramolecular vibrations. Recently, there has been a noticeable trend of using theoretical models to explain how phonons lead to relaxations in SMMs and qubits.[14,15,17–20] Guo et al.[21] have reported that [(Cp^{iPr5})Dy(Cp*)]$^{+}$ displays open magnetic hysteresis up to 80 K. From their theoretical calculations, they deduced that the magnetic relaxation was promoted by the displacements primarily involving the Cp^{iPr5} rings. In some groups, far-infrared (IR) spectroscopy,[13,16,22] Raman spectroscopy,[13] and inelastic neutron scattering[16,23] with an external magnetic field were also used to study the spin–phonon couplings in 3d- and 4f-based mononuclear SMMs. For example, Moseley et al.[13] studied the spin–phonon couplings in [Co(acac)$_2$(H$_2$O)$_2$] and its deuterated analogs with Raman, IR spectroscopies, and inelastic neutron scattering. This work revealed the existence of spin–phonon couplings in some typical transition-metal complexes. As a result, controlling the phonon seems to be a good way to manipulate spin behavior. However, direct evidence of spin–intramolecular vibration coupling through the ac susceptibility or spin decoherence time, for instance, is still lacking.

To obtain direct evidence of spin–intramolecular vibration coupling, the magnetic system should have the same magnetic energy levels and different vibrational energy levels, which is a challenge in chemical synthesis. H/D isotopic labeling does not directly affect the electronic structure of the material and is often used in organic reactions to study the reaction mechanism due to the fact that the mass induced the smaller zero point energy (ZPE) of X–D bond than X–H bond (X is other elements).[24,25] Due to the same size of H and D atom, the H/D isotope effect could not change the crystal lattice,

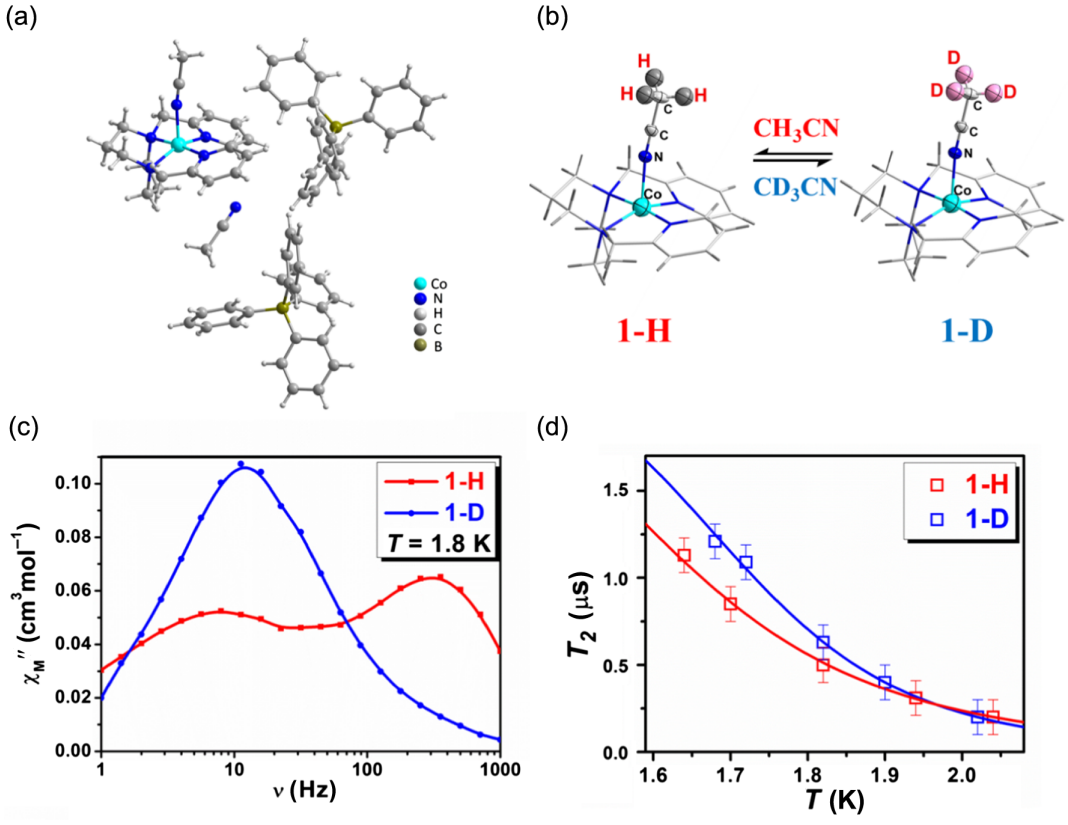

Figure 1. | *The spin dynamic properties tuned through H/D isotopic displacement in complex **1**. (a and b). The structures of complexes **1-H** and **1-D**. (c) Frequency dependence of out-of-phase (χ_M'') ac susceptibilities under 0.6 kOe dc field at 1.8 K for **1-H** and **1-D**. (d) Temperature dependence of spin decoherence times (T_2) for **1-H** and **1-D**.*

DOI: 10.31635/ccschem.020.202000384
Citation: *CCS Chem.* **2020**, 2, 2548–2556
Citation denotes calendar and volume year of first online publication.
Issue Assignment: Volume 3 (2021), Issue 9

but it brings different intramolecular vibration modes (phonon), which provides an excellent opportunity to study the spin–intramolecular vibration coupling in spin dynamics.

Recently, we found a couple of low-spin Co(II) complexes (Figures 1a and 1b),[26] {[CoL](CH$_3$CN)}[BPh$_4$]$_2$·CH$_3$CN (**1-H**) and its deuterated analog {[CoL](CD$_3$CN)}[BPh$_4$]$_2$·CD$_3$CN (**1-D**), exhibiting the rare ON/OFF switching of double spin relaxation behaviors in magnetic relaxation (Figure 1c) as well as the regulation of spin lifetime (Figure 1d) at low temperatures through the H/D isotope effect. Compared with T_1 of Dy(III)-based SMMs,[21] or with T_2 of V=O and Cu(II)-based complexes qubits,[6,9,27,28] our work does not seem exciting, but this research provides the first experimental evidence that the spin dynamics are closely related to specific vibration modes. It further provides new guidance on how to control spin behavior through ultrafast lasers and electric fields.

Experimental Methods

All reagents were commercially available from Innochem Company (Beijing, China) and were used without further purification. Ligand L, complexes **1-H**, **1-D**, Zn(II)-analogs (**2-H** and **2-D**), and doping **1′-H** and **1′-D** were obtained following the reported methods in the literature (Supporting Information Scheme S1).[26] The experimental details about X-ray crystallography, magnetic characterization, Terahertz (THz) spectroscopy analysis, and theoretical calculation are available in the Supporting Information.

Preparation of {[CoL](CH$_3$CN)}[BPh$_4$]$_2$·CH$_3$CN

To a solution of L (0.0532 g, 0.179 mmol) in CH$_3$CN (3 mL) was added [Co(H$_2$O)$_6$](ClO$_4$)$_2$ (0.0632 g, 0.173 mmol) as a solid, yielding a purple solution. The solution was stirred for several minutes, and then a solution of NaBPh$_4$ (0.352 g, 1.03 mmol) in CH$_3$OH (3 mL) was added. A light purple microcrystalline solid immediately precipitates. This solid was collected by vacuum filtration, washed with copious amounts of CH$_3$OH and then Et$_2$O, and dried under air: 0.15 g. Recrystallization from hot CH$_3$CN provided crystals of **1-H** suitable for X-ray crystallography. Anal. Calcd for C$_{70}$H$_{70}$B$_2$CoN$_6$: C, 78.14; H, 6.56; N, 7.81. Found: C, 77.97; H, 6.48; N, 7.68.

Preparation of {[CoL](CD$_3$CN)}[BPh$_4$]$_2$·CD$_3$CN

To a solution of L (0.0532 g, 0.179 mmol) in CD$_3$CN (3 mL) was added [Co(H$_2$O)$_6$](ClO$_4$)$_2$ (0.0632 g, 0.173 mmol) as a solid, yielding a purple solution. The solution was stirred for several minutes, and then a solution of NaBPh$_4$ (0.352 g, 1.03 mmol) in CH$_3$OH (3 mL) was added. A light purple microcrystalline solid immediately precipitates. This solid was collected by vacuum filtration, washed with copious amounts of CH$_3$OH and then Et$_2$O, and dried under air: 0.135 g. Recrystallization from hot CD$_3$CN provided crystals of **1-D** suitable for X-ray crystallography. Anal. Calcd for C$_{70}$H$_{64}$D$_6$B$_2$CoN$_6$: C, 77.71; H, 7.08; N, 7.77. Found: C, 77.80; H, 7.10; N, 7.81.

Preparation of {[ZnL](CH$_3$CN)}[BPh$_4$]$_2$·CH$_3$CN

The above experiment is the same as **1-H**, except that [Zn(H$_2$O)$_6$](ClO$_4$)$_2$ replaces [Co(H$_2$O)$_6$](ClO$_4$)$_2$. Anal. Calcd for C$_{70}$H$_{70}$B$_2$ZnN$_6$: C, 77.68; H, 6.52; N, 7.76. Found: C, 77.67; H, 6.38; N, 7.92.

Preparation of {[ZnL](CD$_3$CN)}[BPh$_4$]$_2$·CD$_3$CN

The above experiment is the same as **1-D**, except that [Zn(H$_2$O)$_6$](ClO$_4$)$_2$ replaces [Co(H$_2$O)$_6$](ClO$_4$)$_2$. Anal. Calcd for C$_{70}$H$_{64}$D$_6$B$_2$ZnN$_6$: C, 77.25; H, 7.04; N, 7.72. Found: C, 77.60; H, 7.11; N, 7.83.

Complexes **1′-H** and **1′-D** were obtained by recrystallization with 5% molar Co: 95% molar Zn in acetonitrile and 5% molar Co: 95% molar Zn in acetonitrile-d3. The dilution ratios were confirmed by inductively coupled plasma atomic emission spectroscopy (ICP-AES) analyses as 5 ± 1%.

Results and Discussions

The two complexes are isostructural (Supporting Information Figure S1 and Table S1), so we will only describe the structure of **1-H** here. The single-crystal X-ray diffraction analysis reveals that the lattice of **1-H** belongs to the orthorhombic space group *P*bca. Each asymmetric unit consists of one Co(II) ion, one ligand L, one coordinated acetonitrile molecule, one free acetonitrile molecule, and two [BPh$_4$]$^-$ anions (Figure 1a). The Co(II) ion is in a distorted tetragonal pyramidal geometry coordinated by four nitrogen atoms from the ligands L and one nitrogen atom from acetonitrile. Among them, N1, N2, N3, and N4 are located on the equatorial plane, and N5 occupies the axial position. The Co–N bond distances range from 1.9450(17) to 2.0773(19) Å, which are comparable with the lengths in other analogous complexes.[17] The packing pattern is displayed in Supporting Information Figure S2. The Co(II)-containing moiety is surrounded by the [BPh$_4$]$^-$ anions. The Co···Co distances range from 12.215 to 13.324 Å. Complex **1-H** further forms a supramolecular network through van der Waals forces. Complexes **1-H** and **1-D** are isostructural with only a slight difference in the angles of N–Co–N (Supporting Information Table S2), which can be attributed to the

DOI: 10.31635/ccschem.020.202000384
Citation: *CCS Chem.* **2020**, 2, 2548–2556
Citation denotes calendar and volume year of first online publication.
Issue Assignment: Volume 3 (2021), Issue 9

different vibrational effects caused by changing $-CH_3$ to $-CD_3$ on the acetonitrile ligand.

The variable-temperature and variable-frequency alternating current (ac) magnetic susceptibilities of **1-H** and **1-D** were carried out with polycrystal samples under low temperature. They revealed no out-of-phase signals for **1-H** and **1-D** without an external direct-current (dc) field. When a small external dc field (>0.2 kOe) is applied, a peak was observed in the frequency-dependent χ_M'' at 2.0 K (Supporting Information Figure S3). The similar slow relaxation behavior was also observed in V(IV)-based complexes, which were dominated by the Raman mechanism or the spin–phonon bottleneck, rather than the double-phonon Orbach relaxation mechanism.[29,30] The relaxation time was investigated in a different magnetic field (0–0.5 T) at 2.0 K. Surprisingly, there are two relaxation processes for **1-H**, while only one process for **1-D** in the dc field range of 0.5–1.0 kOe (Figure 2c). According to our references,[12,31] in the spin–phonon-bottleneck-dominated relaxation process, the relaxation time, τ, is proportional to the crystal size. Hence, the variable-frequency ac magnetic susceptibility of ground samples was measured at 2 K with a different external dc field in the same way (Supporting Information Figure S4). The peaks shifted to high frequency, indicating a faster relaxation. This is a typical characterization of spin–phonon bottleneck. However, two relaxation processes for **1-H**, and only one process for **1-D** in the dc field range of 0.5–1.0 kOe could still be observed (Supporting Information Figure S5), suggesting that the phenomenon stemmed from the intrinsic properties of molecules, rather than the spin–phonon bottleneck. Generally, the spin relaxation is dominated by the spin–nuclear and spin–spin interactions at low fields.[27] However, the spin–nuclear interaction from the H and D was too weak to make such difference in relaxations, due to the long distance between Co(II) ion and H or D in acetonitrile (more than 4.8 Å). It should be noted that all the relaxation processes (direct, Raman, and Orbach processes) except quantum tunneling of magnetization (QTM) are supported by phonons. Thus, the different relaxation behavior observed in 0.5–1.0 kOe can be attributed to the phonons. It is expected that the phonons take part in the relaxation processes with different frequencies for the two complexes.

To get deeper insights on the relaxation mechanism, we measured the ac magnetic susceptibilities of **1-H** and **1-D** under 0.4, 0.6, and 2.0 kOe external dc fields (Figures 2a and 2b and Supporting Information Figures S6–S8).The in-phase and out-of-phase signals for **1-H** and **1-D** showed a slight difference in 0.4 and 2 kOe dc fields, but showed the completely different relaxation patterns under the 0.6 kOe field. The linearity of the ln(τ) versus T^{-1} plots (Supporting Information Figure S9) was fitted by Arrhenius law $\tau = \tau_0 \exp(U_{eff}/k_BT)$. The best-fitted parameters are summarized in Supporting Information Tables S3 and S4. Interestingly, all the τ_0 were in the 10^{-5} s order of magnitude, which is in agreement with the lack of electronic states providing a path for the Orbach mechanism.[14,27,30] With the absence of the Orbach mechanism, the thermal dependence of the relaxation time (τ) has been modeled assuming a direct process dominating at low temperatures and a Raman-like process dominating at high temperatures (eq 1):

$$\tau^{-1} = aT + bT^n \quad (1)$$

where a is the coefficient of the direct process, and b and n are the coefficients of the Raman-like process, respectively. The values of these coefficients only show slight differences, which are within the margin of error (Supporting Information Tables S3 and S4). The parameter n is closed to 3, which is consistent with a system with a strong spin–phonon bottleneck.[12,14,27,30,32,33] When fitting the fast process (area B in Figure 2a) of **1-H** at 0.6 kOe, a QTM process should be considered because of the short temperature-independent relaxation times at low temperatures. This phenomenon would stem from the energy overlap between the unpaired electron and the low-energy barrier vibrations[18,21,33] or the methyl

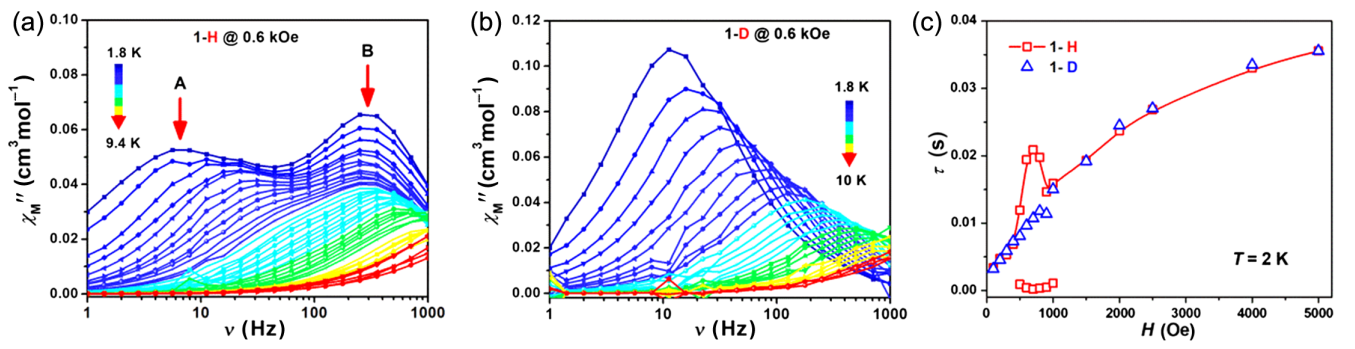

Figure 2 | *(a and b) Frequency dependence of out-of-phase (χ_M'') ac susceptibilities under 0.6 kOe dc field at indicated temperatures for **1-H** and **1-D**, respectively. (c) The isothermal (T = 2 K) relaxation time (τ) extracted from the ac susceptibility measurements for polycrystalline samples of **1-H** and **1-D** at different dc fields.*

DOI: 10.31635/ccschem.020.202000384
Citation: *CCS Chem.* **2020**, 2, 2548–2556
Citation denotes calendar and volume year of first online publication.
Issue Assignment: Volume 3 (2021), Issue 9

tunneling rotations[34] at the given magnetic field. Furthermore, the slow process (area A in Figure 2a) of **1-H** was totally different from that of **1-D** in the same situation, which can only be explained by the intramolecular spin–phonon coupling due only to the difference of H and D in **1-H** and **1-D**.

Interestingly, the extracted energy barriers are ca. 20 cm^{-1} with the Arrhenius law, which is in line with the typical energies of low-energy vibration modes.[35,36] The vibrations distributed on the molecular periphery can largely admix with lattice vibrations. Room temperature time-domain THz spectra were performed in the range of 0.15–1.6 THz (5–55 cm^{-1}) for complexes **1-H** and **2-D** as shown in Supporting Information Figure S10. In the range of 5–20 cm^{-1}, peaks at 6.2, 11.7, and 14.6 cm^{-1} for **1-D** greatly deviated to **1-H** (12.2 and 15.7 cm^{-1}), which can be attributed to the H and D difference in ligand acetonitrile. From the ab initio calculation,[37] the single electron of Co(II) ion is occupied in the d_{z^2} orbital (Supporting Information Figure S13), and the electron density widely spreads to the C≡N of ligand acetonitrile. As a result, the vibration energies of ligand acetonitrile and the coordinated Co–N bond would be influenced by the deuteration considering the ideal vibration energy function of $\nu = \frac{1}{2\pi\sqrt{\mu/k}}$ (μ is reduced mass, and $\mu = (m_1 \times m_2)/(m_1 + m_2)$, $m_D > m_H$, then $\mu_H < \mu_D$). Assuming the relation $U_{eff} = h\omega\alpha/2$ works in this system,[18,20,32,33] the magnetic analysis indicates that the phonons involved in the relaxation mechanism should have a frequency of 26.1 cm^{-1} (0.4 kOe), 11.74 and 11.94 cm^{-1} (0.6 kOe), and 41.2 cm^{-1} (2.0 kOe) for **1-H**, and 26.6 cm^{-1} (0.4 kOe), 30.2 cm^{-1} (0.6 kOe), and 39.8 cm^{-1} (2.0 kOe) for **1-D**, respectively (Supporting Information Figure S10), which are in agreement with the spectroscopic observations. In a word, in this spin 1/2 system, the phonons from the intramolecular vibration modes played crucial roles in the slow magnetization relaxation.

Continuous wave (cw) and pulsed electron paramagnetic resonance (EPR) measurements were performed on a 240 GHz EPR spectrometer at the National High Magnetic Field Laboratory(Tallahassee, FL).[38] The cw-EPR spectra for powder samples of both **1-H** and **1-D** contained three resonance absorption peaks at ca. 7.1, 7.6, and 8.4 T (Supporting Information Figure S11). Fitting the spectrum resulted in the *g*-factors of g_x = 2.408(1), g_y = 2.244(1), and g_z = 2.028(1) and the hyperfine constants of $A_x = A_y$ = 10(1) MHz and A_z = 83(3) MHz for both samples,[30] which were in line with the calculated results (g_x = 2.550, g_y = 2.285, and g_z = 1.983) by complete active space self-consistent field wave functions complemented by N-electron valence second order perturbation theory (CASSCF/NEVPT2).[37] The temperature dependence of quantum coherence time (T_2) of **1-H** and **1-D** was collected using a standard Hahn echo

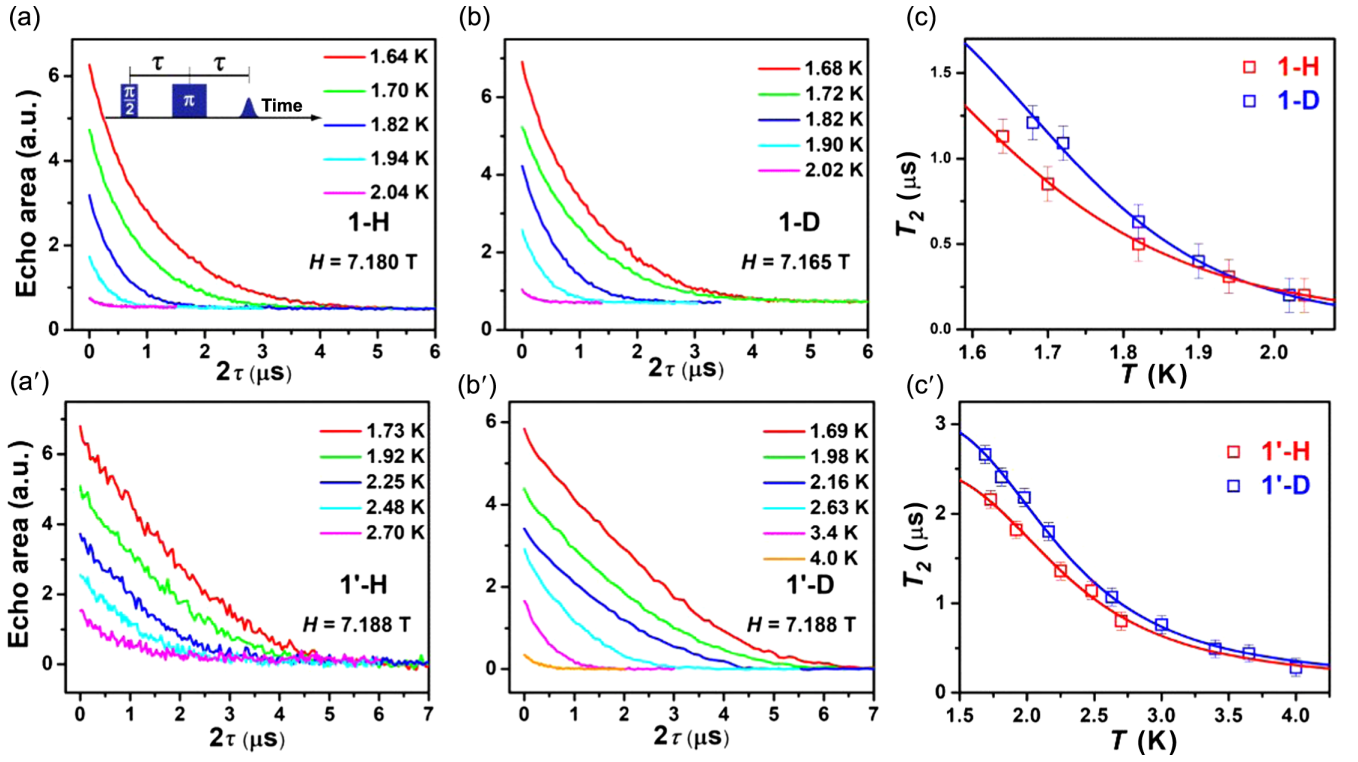

Figure 3 | *(a, b), a′, and b′) Echo signals as a function of 2τ at different temperatures and 240 GHz for **1-H**, **1-D**, **1′-H**, and **1′-D**, respectively. (c and c′) Temperature dependence of 1/T_2. The solid lines are the simulations with the spin bath decoherence model.*

DOI: 10.31635/ccschem.020.202000384
Citation: *CCS Chem.* **2020**, 2, 2548–2556
Citation denotes calendar and volume year of first online publication.
Issue Assignment: Volume 3 (2021), Issue 9

sequence ($\pi/2$-τ-π-τ-echo)[31] in a nonresonating sample holder, with the magnetic field along the *x*-axes (Figures 3a and 3b). T_2 was measured in the temperature range of 1.64–2.04 K (**1-H**) and 1.68–2.02 K (**1-D**), respectively. In the temperature range, the T_2 exhibited a strong temperature dependence and decrease from 1.13 to 0.2 μs (**1-H**) and 1.21 to 0.2 μs (**1-D**), respectively (Figure 3c).

The strong temperature dependence of T_2 suggested that the main decoherence mechanism at higher temperatures is due to the dipolar–dipolar interaction in the electron spin bath. In this system, there were only two levels, $m_s = -1/2$ and $m_s = +1/2$. At the high field of 7.17 ± 0.02 T, single spin flips were highly suppressed, and the spin bath fluctuations were dominated by energy-conserving spin flip-flop processes.[10,11] For a quantitative analysis, the temperature dependence of $1/T_2$ is fitted by a spin bath decoherence model,[10,11,20,39]

$$\frac{1}{T_2} = \frac{C}{(1+e^{T_{Ze}/T})(1+e^{-T_{Ze}/T})} + \Gamma_{res} \qquad (2)$$

where C is a temperature-independent parameter, T_{Ze} the temperature corresponding to Zeeman energy, and Γ_{res} the residual relaxation rate due to the temperature-independent decoherence source. T_{Ze} is obtained as 25.6 K for **1-H** and 18.4 K for **1-D**, which were close to the Zeeman energy of 11.5 K (240 GHz), strongly supporting the decoherence mechanism caused by the Co spin bath fluctuation. The resulting residual relaxation rate Γ_{res} was 0.45 μs^{-1} for **1-H** and 0.41 μs^{-1} K for **1-D**, corresponding to $T_2 \sim 2$ μs. This residual decoherence is mainly due to the hyperfine coupling of ^{59}Co (100% natural abundance), and represents the decoherence time expected for a highly diluted sample.

To further investigate the intrinsic sources of spin decoherence, the T_2 times of doped materials **1′-H** and **1′-D** with diamagnetic Zn(II) ions (Co:Zn = 5:95 mole ratio) were measured in the temperature range of 1.73–2.70 K (**1′-H**) and 1.69–4.00 K (**1′-D**) (Figures 3a′ and 3b′). The T_2 times also exhibited strong temperature dependence and decrease from 2.16 to 0.8 μs (**1′-H**) and 2.66 to 0.28 μs (**1′-D**) (Figure 3c′). Equation. 2 was also used to express the temperature dependence of $1/T_2$ with T_{Ze} set to the Zeeman energy of 11.5 K (240 GHz). Very good fittings were obtained, indicating that the spin bath decoherence model described the decoherence mechanism of **1′-H** for **1′-D** very well. The resulting residual relaxation rate Γ_{res} was 0.24 μs^{-1} for **1′-H** and 0.38 μs^{-1} K for **1′-D**, corresponding to $T_2 \sim 4$ and 3 μs, respectively, in the same order as the undoped samples. The doped materials **1′-H** and **1′-D** were also studied on the (pulsed) X-band EPR equipment (Supporting Information Figure S12). Fitting the cw-EPR spectrum results in the *g*-factors of $g_x = 2.408(1)$, $g_y = 2.244(1)$, and $g_z = 2.028(1)$ and the hyperfine constants of $A_x = A_y = 10(1)$ MHz and $A_z = 83(3)$ MHz for both samples showed good agreement with the high-field EPR spectrum. No obvious hyperfine interaction between the nuclear spins of N atoms and the electron spin of Co ions was observed. However, no spin echo signals were detected for both samples even at 4.0 K, indicating that the spin lifetime was too short to measure. Generally, the T_2 time is longer under a high magnetic field, because the single spin flips are highly suppressed by the magnetic field. Now, the T_2 of **1′-D** was only 0.28 μs at 4 K under a 7.188 T high magnetic field, which is easily quenched by active spin flips under the low magnetic field (~0.3 T).[40]

It is very interesting to discuss why the T_2 of **1-D** is longer than that of **1-H** at low temperatures. Since the Γ_{res} values were very close for the two complexes, the difference of decoherence time is highly likely to originate from the temperature-dependent source, which contains the spin–spin dipolar interaction, spin–solvent electrostatic interaction, spin–nuclear interaction, and spin–vibration interaction (see Supporting Information Equation S2). After an in-depth analysis (see Part Four in Supporting Information), we concluded that the spin–vibration interaction was the main source of the difference in spin decoherence time at low temperatures. The vibration energies of ligand acetonitrile and the coordinated Co–N bond in **1-D** were larger than **1-H**. Furthermore, the deuterated methyl groups underwent tunneling at a much lower frequency than protiated methyl.[41] As a result, the rotational and vibrational barrier was lower for **1-H**, which led to the faster decoherence that we observed. Since replacing the C–H with C–D bond largely influenced the spin–phonon interactions of studied molecules, we conclude that spin–phonon (vibration and rotation) coupling at low temperatures is the dominant decoherence mechanism for above studied complexes.

Recently, Zadrozny et al.[42] reported an atomic clock qubit, a low-spin Co(II) ion located in a rigid porphyrin ligand ([CoTPP]), showing that T_2 increases with the decrease in temperature, from 1.96(1) μs at 15 K to 13.74(9) μs at 5 K. Both the T_2 and temperature were predominant compared with our complexes. According to our calculations, the electronic structure is similar and the single electron is also occupied in the d_{z^2} orbital. However, no ligand was located in the d_{z^2} orbital, avoiding the vibration which accelerates the spin decoherence. Furthermore, Xu et al.[43] reported a similar structural low-spin Co(II) qubit with high symmetry (C_{4h}), demonstrating spin echo in the temperature range from 5 to 25 K. And the spin life at 5 K can reach 900 ns, which is much longer than our complexes. This suggests that the symmetry of molecular structure plays an important role in quantum coherence.[12] Above all, using high symmetry and rigid ligands is an effective strategy to lengthen a spin–spin relaxation time.

To prove that the difference in electron structure between **1-H** and **1-D** is negligible, we conduct a

DOI: 10.31635/ccschem.020.202000384
Citation: *CCS Chem.* **2020**, 2, 2548–2556
Citation denotes calendar and volume year of first online publication.
Issue Assignment: Volume 3 (2021), Issue 9

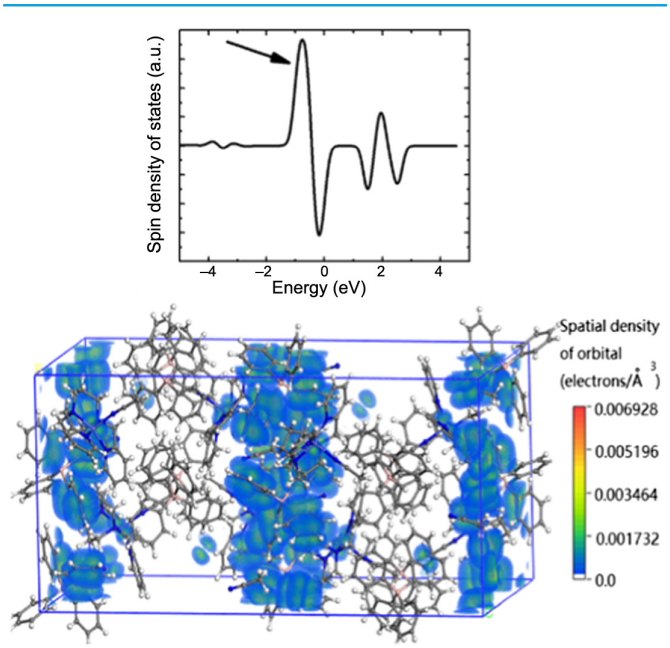

Figure 4 | *Spatial distribution of the Co spin state. The arrow in the upper panel indicates the position of the shown orbital in the spin density of states.*

computational study of the electronic structure of the two complexes. In Figure 4, we plot the spatial distribution of the spin state of Co by using the first-principles calculation with Cambridge Sequential Total Energy Package (CASTEP).[44] We can see that the Co spin state is extended to cover CH_3 or CD_3 groups, but the spin state is still limited with a certain boundary local to the clusters. The replacement of H with D can affect the decoherence rate of the Co spins from two aspects: (1) The H nuclear spins ($I = 1/2$), which can contribute to the spin bath for decoherence of the Co spins, are replaced with D nuclear spins ($I = 1$). (2) The frequencies of vibrations involving the replaced atoms are lowered due to the larger mass of deuterium nuclei. Thus, in the spin bath model, we should consider (1) the change of the nuclear spins when replacing H with D; (2) the change of the fluctuations of the spin bath due to the different vibration frequencies. The fluctuations of the spin bath are also influenced by the vibrations of CH_3 or CD_3 groups, which can continuously disturb the magnetic interactions between the Co spins and the H or D nuclear spins (the hyperfine interactions), since H or D nuclei are at the boundaries of the Co spin state. By taking all the factors above into consideration, the spin bath model can be rewritten as $1/T_2 = \Gamma_1 + \Gamma_2 + \Gamma'_{res}$, where Γ_1 and Γ_2 are contributions from mechanisms (a) and (b), and Γ'_{res} is the contribution from all other sources. Here, Γ'_{res} is not changed by replacing H with D, but it may be temperature dependent. Since the nuclear spin is $I = 1/2$ for H and $I = 1$ for D, we have

$$\Gamma_1 = C_1 P_{m_S=-1/2} P_{m_S=1/2} \text{ for } \mathbf{1\text{-}H}$$

and

$$\Gamma_2 = C_2 (P_{m_S=-1} P_{m_S=0} + P_{m_S=1} P_{m_S=0} + P_{m_S=-1} P_{m_S=1}) \text{ for } \mathbf{1\text{-}D},$$

where $P_{m_S} = \exp(-\varepsilon_{m_S}/k_B T)/\sum_{m'_S} \exp(-\varepsilon_{m'_S}/k_B T)$ is the probability of the nuclear spin being in state m_S. Since the spin level gap (the Zeeman energy) is about 0.006 K for H and 0.002 K for D, which are much smaller than the investigated temperature range (1–4 K), Γ_1 is almost temperature independent. On the other hand, since the fluctuations caused by the vibrations are proportional to the intensity of the related phonons, we have $\Gamma_2 = D/[\exp(h\nu/k_B T)-1]$, where ν is the frequency of phonons. Because $h\nu/k_B$ is in the range of 10–100 K, Γ_2 will exhibit an evident increase as the temperature increases.

Conclusions

We studied two low-spin Co(II) complexes showing the slow magnetic relaxation and quantum coherence at low temperatures. The ac magnetometry indicated that the slow magnetic relaxation mechanism was closely related to the intramolecular vibration/rotation, namely the spin–phonon coupling. High-frequency pulsed EPR studies showed that spin–spin relaxation times of deuterated samples were longer than protiated samples at low temperatures. With the distinct spin dynamics behaviors of the two complexes, and supported by theoretical calculation results, we have provided an experimental case proving that the intramolecular vibrations and rotations play key roles in the spin dynamics of qubits. A rigid ligand environment would increase the energy of vibration modes, which can reduce the spin–phonon coupling and prolong the spin relaxation times. As we all know optical and electric fields can resonantly excite special vibration modes, and our research provides new guidance for ultrafast and electrical control of spin behavior.

Supporting Information

Supporting Information is available.

Conflict of Interest

There is no conflict of interest to report.

Funding Information

This work was supported by the Major State Basic Research Development Program (nos. 2017YFA0303203 and 2018YFA0306004), the National Natural Science Foundation of China (nos. 21571097, 21973038,

21701046, and 21601005), the Fundamental Research Funds for the Central Universities (no. 2018KFYXKJC010), and the Young Elite Scientist Sponsorship Program of the China Association of Science and Technology (no. YESS20150011). A portion of this work was performed at the National High Magnetic Field Laboratory, which is supported by the National Science Foundation through NSF/DMR-1157490, 1644779 and the State of Florida.

References

1. Benelli, C; Gatteschi, D. *Introduction to Molecular Magnetism: From Transition Metals to Lanthanides*; Wiley: New York, **2015**.
2. Moreno-Pineda, E.; Godfrin, C.; Balestro, F.; Wernsdorfer, W.; Ruben, M. Molecular Spin Qudits for Quantum Algorithms. *Chem. Soc. Rev.* **2018**, *47*, 501–513.
3. Atzori, M.; Sessoli, R. The Second Quantum Revolution: Role and Challenges of Molecular Chemistry. *J. Am. Chem. Soc.* **2019**, *141*, 11339–11352.
4. Guo, L.; Gu, X.; Zhu, X.; Sun, X. Recent Advances in Molecular Spintronics: Multifunctional Spintronic Devices. *Adv. Mater* **2019**, *31*, e1805355.
5. Ladd, T. D.; Jelezko, F.; Laflamme, R.; Nakamura, Y.; Monroe, C.; O'Brien, J. L. Quantum Computers. *Nature* **2010**, *464*, 45–53.
6. Zadrozny, J. M.; Niklas, J.; Poluektov, O. G.; Freedman, D. E. Millisecond Coherence Time in a Tunable Molecular Electronic Spin Qubit. *ACS Cent. Sci.* **2015**, *1*, 488–492.
7. Wernsdorfer, W.; Caneschi, A.; Sessoli, R.; Gatteschi, D.; Cornia, A.; Villar, V.; Paulsen, C. Effects of Nuclear Spins on the Quantum Relaxation of the Magnetization for the Molecular Nanomagnet Fe_8. *Phys. Rev. Lett.* **2000**, *84*, 2965–2968.
8. Eaton, S. S.; Eaton, G. R. Relaxation Times of Organic Radicals and Transition Metal Ions. *Biol. Magn. Reson.* **2002**, *19*, 29–129.
9. Yu, C. J.; Graham, M. J.; Zadrozny, J. M.; Niklas, J.; Krzyaniak, M. D.; Wasielewski, M. R.; Poluektov, O. G.; Freedman, D. E. Long Coherence Times in Nuclear Spin-Free Vanadyl Qubits. *J. Am. Chem. Soc.* **2016**, *138*, 14678–14685.
10. Takahashi, S.; Hanson, R.; van Tol, J.; Sherwin, M. S.; Awschalom, D. D. Quenching Spin Decoherence in Diamond Through Spin Bath Polarization. *Phys. Rev. Lett.* **2008**, *101*, 047601.
11. Kutter, C.; Moll, H. P.; van Tol, J.; Zuckermann, H.; Maan, J. C.; Wyder, P. Electron-Spin Echoes at 604 GHz Using Far Infrared Lasers. *Phys. Rev. Lett.* **1995**, *74*, 2925–2928.
12. Li, J.; Yin, L.; Xiong, S.-J.; Wu, X.-L.; Yu, F.; Ouyang, Z.-W.; Xia, Z.-C.; Zhang, Y.-Q.; van Tol, J.; Song, Y.; Wang, Z. Controlling Electron Spin Decoherence in Nd-Based Complexes via Symmetry Selection. *iScience* **2020**, *23*, 100926.
13. Moseley, D. H.; Stavretis, S. E.; Thirunavukkuarasu, K.; Ozerov, M.; Cheng, Y.; Daemen, L. L.; Ludwig, J.; Lu, Z.; Smirnov, D.; Brown, C. M.; Pandey, A.; Ramirez-Cuesta, A. J.; Lamb, A. C.; Atanasov, M.; Bill, E.; Neese, F.; Xue, Z.-L. Spin–Phonon Couplings in Transition Metal Complexes with Slow Magnetic Relaxation. *Nat. Commun.* **2018**, *9*, 2572.
14. Lunghi, A.; Totti, F.; Sanvito, S.; Sessoli, R. Intra-Molecular Origin of the Spin-Phonon Coupling in Slow-Relaxing Molecular Magnets. *Chem. Sci.* **2017**, *8*, 6051–6059.
15. Albino, A.; Benci, S.; Tesi, L.; Atzori, M.; Torre, R.; Sanvito, S.; Sessoli, R.; Lunghi, A. First-Principles Investigation of Spin–Phonon Coupling in Vanadium-Based Molecular Spin Quantum Bits. *Inorg. Chem.* **2019**, *58*, 10260–10268.
16. Moseley, D. H.; Stavretis, S. E.; Zhu, Z.; Guo, M.; Brown, C. M.; Ozerov, M.; Cheng, Y.; Daemen, L. L.; Richardson, R.; Knight, G.; Thirunavukkuarasu, K.; Ramirez-Cuesta, A. J.; Tang, J.; Xue, Z.-L. Inter-Kramers Transitions and Spin–Phonon Couplings in a Lanthanide-Based Single-Molecule Magnet. *Inorg. Chem.* **2020**, *59*, 5218–5230.
17. Lunghi, A.; Sanvito, S. How Do Phonons Relax Molecular Spins? *Sci. Adv.* **2019**, *5*, eaax7163.
18. Lunghi, A.; Totti, F.; Sessoli, R.; Sanvito, S. The Role of Anharmonic Phonons in Under-Barrier Spin Relaxation of Single Molecule Magnets. *Nat. Commun.* **2017**, *8*, 14620.
19. Mirzoyan, R.; Hadt, R. G. The Dynamic Ligand Field of a Molecular Qubit: Decoherence Through Spin–Phonon Coupling. *Phys. Chem. Chem. Phys.* **2020**, *22*, 11249–11265.
20. Escalera-Moreno, L.; Suaud, N.; Gaita-Ariño, A.; Coronado, E. Determining Key Local Vibrations in the Relaxation of Molecular Spin Qubits and Single-Molecule Magnets. *J. Phys. Chem. Lett.* **2017**, *8*, 1695–1700.
21. Guo, F.-S.; Day, B. M.; Chen, Y.-C.; Tong, M.-L.; Mansikkamäki, A.; Layfield, R. A. Magnetic Hysteresis up to 80 Kelvin in a Dysprosium Metallocene Single-Molecule Magnet. *Science* **2018**, *362*, 1400–1403.
22. Rechkemmer, Y.; Breitgoff, F. D.; van der Meer, M.; Atanasov, M.; Hakl, M.; Orlita, M.; Neugebauer, P.; Neese, F.; Sarkar, B.; van Slageren, J. A Four-Coordinate Cobalt(II) Single-Ion Magnet with Coercivity and a Very High Energy Barrier. *Nat. Commun.* **2016**, *7*, 10467.
23. Stavretis, S. E.; Moseley, D. H.; Fei, F.; Cui, H. H.; Cheng, Y.; Podlesnyak, A. A.; Wang, X.; Daemen, L. L.; Hoffmann, C. M.; Ozerov, M.; Lu, Z.; Thirunavukkuarasu, K.; Smirnov, D.; Chang, T.; Chen, Y. S.; Ramirez-Cuesta, A. J.; Chen, X. T.; Xue, Z. B. Spectroscopic Studies of the Magnetic Excitation and Spin-Phonon Couplings in a Single-Molecule Magnet. *Eur. J. Chem.* **2019**, *25*, 15846–15857.
24. Wade, D. Deuterium Isotope Effects on Noncovalent Interactions between Molecules. *Chem. Biol. Interact.* **1999**, *117*, 191–217.
25. Wang, Y.; Olankitwanit, A.; Rajca, S.; Rajca, A. Intramolecular Hydrogen Atom Transfer in Aminyl Radical at Room Temperature with Large Kinetic Isotope Effect. *J. Am. Chem. Soc.* **2017**, *139*, 7144–7147.
26. Fox, D. C.; Fiedler, A. T.; Halfen, H. L.; Brunold, T. C.; Halfen, J. A. Electronic Structure Control of the Nucleophilicity of Transition Metal-Thiolate Complexes: An Experimental and Theoretical Study. *J. Am. Chem. Soc.* **2004**, *126*, 7627–7638.

27. Atzori, M.; Morra, E.; Tesi, L.; Albino, A.; Chiesa, M.; Sorace, L.; Sessoli, R. Quantum Coherence Times Enhancement in Vanadium(IV)-Based Potential Molecular Qubits: The Key Role of the Vanadyl Moiety. *J. Am. Chem. Soc.* **2016**, *138*, 11234–11244.
28. Bader, K.; Dengler, D.; Lenz, S.; Endeward, B.; Jiang, S. D.; Neugebauer, P.; van Slageren, J. Room Temperature Quantum Coherence in a Potential Molecular Qubit. *Nat. Commun.* **2014**, *5*, 5304.
29. Tesi, L.; Lucaccini, E.; Cimatti, I.; Perfetti, M.; Mannini, M.; Atzori, M.; Morra, E.; Chiesa, M.; Caneschi, A.; Sorace, L.; Sessoli, R. Quantum Coherence in a Processable Vanadyl Complex: New Tools for the Search of Molecular Spin Qubits. *Chem. Sci.* **2016**, *7*, 2074–2083.
30. Abragam, A.; Bleaney, B. *Electron Paramagnetic Resonance of Transition Ions*; Oxford University Press: Oxford, UK, **2012**.
31. Schweiger, A.; Jeschke, G. *Principles of Pulse Electron Paramagnetic Resonance*; Oxford University Press: Oxford, UK, **2001**.
32. Atzori, M.; Benci, S.; Morra, E.; Tesi, L.; Chiesa, M.; Torre, R.; Sorace, L.; Sessoli, R. Structural Effects on the Spin Dynamics of Potential Molecular Qubits. *Inorg. Chem.* **2018**, *57*, 731–740.
33. Atzori, M.; Tesi, L.; Benci, S.; Lunghi, A.; Righini, R.; Taschin, A.; Torre, R.; Sorace, L.; Sessoli, R. Spin Dynamics and Low Energy Vibrations: Insights from Vanadyl-Based Potential Molecular Qubits. *J. Am. Chem. Soc.* **2017**, *139*, 4338–4341.
34. Eaton, G. R.; Eaton, S. S. Solvent and Temperature Dependence of Spin Echo Dephasing for Chromium(V) and Vanadyl Complexes in Glassy Solution. *J. Magn. Reson.* **1999**, *136*, 63–68.
35. Tesi, L.; Lunghi, A.; Atzori, M.; Lucaccini, E.; Sorace, L.; Totti, F.; Sessoli, R. Giant Spin-Phonon Bottleneck Effects in Evaporable Vanadyl-Based Molecules with Long Spin Coherence. *Dalton Trans.* **2016**, *45*, 16635–16643.
36. Chen, H.; Pope, T.; Wu, Z.-Y.; Wang, D.; Tao, L.; Bao, D.-L.; Xiao, W.; Zhang, J.-L.; Zhang, Y.-Y.; Du, S.; Gao, S.; Pantelides, S. T.; Hofer, W. A.; Gao, H.-J. Evidence for Ultralow-Energy Vibrations in Large Organic Molecules. *Nano Lett.* **2017**, *17*, 4929–4933.
37. Karlström, G.; Lindh, R.; Malmqvist, P.-Å.; Roos, B. O.; Ryde, U.; Veryazov, V.; Widmark, P.-O.; Cossi, M.; Schimmelpfennig, B.; Neogrady, P.; Seijo, L. MOLCAS: A Program Package for Computational Chemistry. *Comput. Mater. Sci.* **2003**, *28*, 222–239.
38. Morley, G. W.; Brunel, L.-C.; van Tol, J. A Multifrequency High-Field Pulsed Electron Paramagnetic Resonance/Electron-Nuclear Double Resonance Spectrometer. *Rev. Sci. Instrum.* **2008**, *79*, 064703.
39. Takahashi, S.; van Tol, J.; Beedle, C. C.; Hendrickson, D. N.; Brunel, L. C.; Sherwin, M. S. Coherent Manipulation and Decoherence of S = 10 Single-Molecule Magnets. *Phys. Rev. Lett.* **2009**, *102*, 087603.
40. Takahashi, S.; Tupitsyn, I. S.; van Tol, J.; Beedle, C. C.; Hendrickson, D. N.; Stamp, P. C. E. Decoherence in Crystals of Quantum Molecular Magnets. *Nature* **2011**, *476*, 76–79.
41. Hoch, M. J. R.; Bovey, F. A.; Davis, D. D.; Douglass, D. C.; Falcone, D. R.; McCall, D. W.; Slichter, W. P. Nuclear Magnetic Resonance in Poly(vinyl acetate). *Macromolecules* **1971**, *4*, 712–715.
42. Zadrozny, J. M.; Gallagher, A. T.; Harris, T. D.; Freedman, D. E. A Porous Array of Clock Qubits. *J. Am. Chem. Soc.* **2017**, *139*, 7089–7094.
43. Xu, M.-X.; Liu, Z.; Dong, B.-W.; Cui, H.-H.; Wang, Y.-X.; Su, J.; Wang, Z.; Song, Y.; Chen, X.-T.; Jiang, S.-D.; Gao, S. Single-Crystal Study of a Low Spin Co(II) Molecular Qubit: Observation of Anisotropic Rabi Cycles. *Inorg. Chem.* **2019**, *58*, 2330–2335.
44. Clark, S. J.; Segall, M. D.; Pickard, C. J.; Hasnip, P. J.; Probert, M. J.; Refson, K.; Payne, M. C. First Principles Methods Using CASTEP. *Z. Kristallogr.* **2005**, *220*, 567–570.

DOI: 10.31635/ccschem.020.202000384
Citation: *CCS Chem.* **2020**, 2, 2548–2556
Citation denotes calendar and volume year of first online publication.
Issue Assignment: Volume 3 (2021), Issue 9